ION AND PLASMA SOURCES

GENERATION OF A PLASMA CLOT IN A MULTICHANNEL INJECTOR OF A PULSED PLASMA ACCELERATOR

© 2025 V.E. Zavalova*, A.A. Kozlov, A.V. Kozlov, Yu.V. Karpushin, V.P. Polischuk, A.N. Gusev, M.A. Shurupov

Joint Institute for High Temperatures of the Russian Academy of Sciences (JIHT RAS), Moscow, Russia

**e-mail: zavalova@fites.ru*

Received October 26, 2024
Revised November 27, 2024
Accepted December 14, 2024

Abstract. The article presents experimental studies of the plasma clot formation process in the injector, which is the initial section of a coaxial accelerator. Design solutions, experimental setup, and measurement results are described. The design features of the injector include controlled supply of the working gas through electrodynamic valves uniformly installed around the circumference of the outer electrode, a profiled inner electrode, and a solenoid located outside the injector. The diagnostic system included measuring currents and voltages in the discharge circuit and the solenoid circuit; high-speed video filming; measuring plasma parameters using spectral methods and a triple Langmuir probe. Video footage of the plasma clot formation, results of current and voltage measurements, temperature, and electron concentration are presented; the influence of the external magnetic field on the processes in the injector is considered.

Keywords: *pulse plasma accelerator, gas injection, electrodynamic valve*

DOI: 10.31857/S03672921250110e1

1. INTRODUCTION

Interest in pulsed plasma accelerators (PPA) is due to the constant expansion of their practical applications, among which the most relevant are the deposition of various coatings [1, 2]; X-ray sources [3-4]; space plasma guns [5], thermonuclear fusion technology [6 - 9] and others.

The achievable plasma parameters in PPA vary over a wide range: flow velocities up to 10^3 km/s; electron densities above 10^{17} m^{-3}; pulse duration from 1 μs to 1 ms; electron temperature from 1 eV to 1 keV. Recently, the use of PPA for injecting plasma bunches into a thermonuclear reactor has been considered; for these purposes, bunches with a mass of about 20 mg and an energy content of more than 100 kJ are of interest.

The complexity of the task for theoretical analysis and mathematical modeling of processes in plasma bunches is determined by their nonlinear characteristics, the complexity of flow geometry, and

pulsed energy input [10-12]. Increasing the energy content of plasma is hindered mainly by plasma contamination from impurities coming from the walls. An external magnetic field reduces the negative impact of this effect [13]. Due to the difficulty of theoretical analysis of these physical processes, the role of experimental studies of IPU on full-scale test benches increases. It is advisable to separately study the defining element of the IPU – the multi-channel injector (MCI), which is the initial section of the coaxial plasma accelerator. In the MCI, working gas (hydrogen) is injected through electrodynamic valves, ionized, and an initial plasma bunch is formed.

This article discusses the design of the MCI, which allows simultaneous use of up to six valves. The aim of this work was an experimental study of plasma bunch formation in the MCI and assessment of the external magnetic field's influence on its characteristics.

2. DESCRIPTION OF THE TEST BENCH AND EXPERIMENTAL SETUP

A photograph of the MCI model is presented in Fig.1. In the foreground is the output viewing window (flange) – which is also the output section of the MCI, which will subsequently be connected to the IPU. Six hydrogen supply valves are visible around the MCI. Behind the valves is a current collector for connecting cables from the capacitive storage (CS1), which supplies voltage to the discharge gap. The capacity of CS1 was 12 μF, with a maximum charging voltage of 50 kV (working voltage – 25 kV). Above the output flange of the MCI is a cable collector for connecting the capacitive storage CS2 to the external solenoid. The capacity of CS2 was 96 μF, with a charging voltage of up to 40 kV. The capacitive storages were triggered with specified delays using solid-state dischargers (SSD) described in [14]. Before the experiment, a two-stage evacuation of the MCI was performed using a fore-vacuum and turbomolecular pumps to a residual pressure of ~ 0.1 mPa.

Figure 2 shows a sketch of the MCI design in longitudinal and transverse sections. Residual gas was pumped out through a through hole in the central electrode (cathode) *7*. Hydrogen was injected from valves *3* into the gap between the coaxial electrodes *1* and *7*. The electrodes were separated by an insulator with a developed surface *2*, which prevented breakdown along it. Six valves *3* are evenly distributed on the outer electrode, which fundamentally distinguishes this design from other injectors, in which gas entered through a single central valve [3-10].

Gas injection occurred as follows: first, hydrogen entered through channels into the mixing ring *12*, and from there through a 1.1 mm wide slit into the discharge gap at an acute angle to the outer electrode. Opposite the mixing ring slit, the electrode surface was profiled, which facilitated the swirling of jets flowing from the valves *3*. The diameter of the central and outer electrodes is 70 and 150 mm respectively; the electrodes were made of stainless steel. The outer electrode *1* was a cylinder

with a wall thickness of 2 mm, on which a solenoid *1* was wound, reinforced with a fiberglass bandage *6* for strength. The length of the central electrode *7* was 320 mm. The distance from the valve nozzle to the output flange was 366 mm, to the output section of the central electrode - 190 mm. Electrodynamic valves *3* were used, the design of which was borrowed from works [8, 9]. The difference in response time of different valves, which was ~ 100 μs, was equalized by setting delay times for their launch; the valves remained open for ~1 ms. After launching the electrodynamic valves with a predetermined delay time, depending on the valves used, the TTR triggered, supplying voltage from EN1 to the discharge gap, with the outer electrode (anode) being grounded.

The amount of gas entering the valves from a cylinder with an initial pressure of ~3 MPa was regulated by valves. After the experiment, the pressure in the system decreased by ~0.1-0.3 MPa. The volume of the MKI chamber is about 8 l; the gas volume in the electrodynamic valve is 98 ml. The mass of hydrogen entering the discharge chamber was estimated from the pressure change in the sub-valve volume. For one valve, this mass was on average about 8 mg (or $2.5 \cdot 10^{21}$ hydrogen molecules), for six valves - approximately six times more.

Solenoid *11* created a longitudinal magnetic field in the interelectrode gap, which influenced the formation of the plasma clot. The inner diameter of the solenoid was 152 mm, its length was 74 mm, the solenoid winding was made with copper bus in three turns with four leads; the solenoid inductance was 0.82 μH.

In our experiments, the discharge current and voltage, solenoid current were recorded, high-speed video recording was conducted, and plasma parameters were measured. Currents were measured by Rogowski coils, voltage - by an oscilloscope using a voltage divider. Plasma parameters were measured by a triple Langmuir probe (TLP) and spectral methods. To reduce electromagnetic interference, fiber optic data transmission channels and shielding of measuring equipment were used in most cases.

The diagnostic system is explained in Fig. 3. Probe measurements were conducted simultaneously with video recording. The observation plane of the plasma clot was chosen near the outlet section of the valves; it was optically aligned with the receiving matrix of the high-speed Phantom VEO-710 camera. The basic video recording mode: frame size 64×64 pixels, speed - 430 thousand frames per second, exposure - 1.9 μs.

The advantage of TLP is the ability to continuously record local values of electron temperature and density throughout the entire pulse. The TLP connection scheme shown in Fig.3 is similar to the scheme used in work [15]. A vacuum input through a viewing window was made for simultaneous measurements of local plasma parameters and visualization of plasma formation. The molybdenum

electrodes of the TLP protruding into the plasma flow were soldered to high-voltage copper wires . The length of the TZL electrodes is 15 mm, their diameter is 1 mm, the distance between them is 3 mm.

When processing probe measurements, the temperature T_e and electron concentration n_e the following relationships were used [15]:

$$k_B T_e = \frac{e(V1-V_3)_{ln2}}{} \quad (1)$$

$$n_e = \frac{I_1}{0.61 \cdot S \cdot e \cdot \sqrt{k_B T_e / m_i}} \cdot \frac{\exp\left(-\frac{e(V_1-V_3)}{k_B T_e}\right)}{1-\exp\left(-\frac{e(V_1-V_3)}{k_B T_e}\right)} \quad (2)$$

where S is the surface area of the probe that collects current from the plasma, k_B is the Boltzmann constant, e is the electron charge, m_i is the ion mass, I_1 is the ion saturation current, equal to the ratio $(V_1 - V_2)/R$, where R is the resistance in the measuring circuit; $V_1 - V_2$ is the bias voltage applied to electrodes *1* and *2* ; $V_1 - V_3$ is the potential difference between electrode *1* and the floating potential of electrode *3* . The coefficient 0.61 in the denominator of formula (2) accounts for the difference in electron concentration at the outer boundary of the space charge layer and on the probe surface [16].

In spectral measurements, a SOLAR *3* M266 monochromator was used (Fig. 3). Plasma radiation was collected by a collimator with a diameter of 15 mm. Single-frame registration was carried out through the main output port using the built-in Toshiba1304 camera (a photodiode array with 3648 pixels, pixel size 8 ×200 μm). An external synchronization pulse with a rise time of ~1 μs was used to synchronize the measurements. A high-speed Phantom VEO710 camera (7 Gpixels/s) recorded the plasma spectrum through an additional output port of the monochromator.

The electron temperature was estimated by the relative intensity of the Balmer series lines H_α and H_β. In these experiments, a diffraction grating of 300 lines/mm was used, covering the spectral range $\Delta\lambda$ =370 nm and providing a resolution and inverse linear dispersion of 0.4 nm and 12.6 nm/mm, respectively. The electron temperature calculation was carried out using the known formula (3) [17]

$$T_e = \frac{\Delta E}{\left[ln\left(\frac{I_1 f_2 g_2 \cdot \lambda_1^{\,3}}{I_2 f_1 g_1 \cdot \lambda_2^{\,3}}\right)\right] \cdot k_B} \quad (3)$$

where I_1 and I_2 – intensities of lines H_α and H_β ; λ_1 =656.3nm and λ_2 = 486.1 nm - wavelengths of lines H_α and H_β ; f_1 =0.641 and f_2 =0.119 – total oscillator strengths for the emissions of lines H_α and H_β [18]; g_1 =18 and g_2 = 32 – statistical weights of levels with principal quantum numbers $n=n_1=3$ and $n=n_2=4$, ΔE= 0.66 eV – the difference in their energies.

The electron concentration was determined through the relationship between the emission coefficient and the spectral line width α , which is normalized by the condition $\int_{-\infty}^{+\infty} S(\alpha)d\alpha = 1$, where $\alpha = 2.61\ \Delta\lambda\ e\ (n_e)^{2/3}$ establishes the relationship between electron concentration and $\Delta\lambda$ (distance from the center of the perturbed line). According to the methodology described in [16], from the experimentally found profile we obtained α , calculated the line broadening $\Delta\lambda$, and then determined the electron concentration. For the H_β line, linear Stark broadening is applicable, denoted as $\Delta\lambda_s$. This value is calculated in the general case taking into account instrumental broadening $\Delta\lambda_a$. Since a diffraction grating of 1200 lines/mm was used for broadening measurements in the monochromator, providing a resolution of ~0.1 nm; then with a dispersion of 3.18 nm/mm, and an entrance slit width of 5 μm, the instrumental broadening was $\Delta\lambda_a = 1.6 \cdot 10^{-2}$ nm. This value is two orders of magnitude less than the characteristic value of the measured half-width of the H_β line $\Delta\lambda \sim 1.2$ nm. Therefore, for n_e the calculation formula from [19] was applied

$$n_e = 10^{13} \cdot \Delta\lambda_S^{3/2}[C_o(T) + C_1(T) \cdot \ln(\Delta\lambda_S)], \quad \text{cm}^{-3}, \tag{4}$$

where $\Delta\lambda_s \sim \Delta\lambda$, and the values of constants $C_0 = 36.56$ and $C_1 = -1.45$ corresponded to the ion temperature, which due to the short duration of the discharge can be assumed equal to the ambient temperature.

3. EXPERIMENTAL RESULTS

The experiment was conducted according to the following scheme. After launching the electrodynamic valves, the TTR was triggered after ~0.4 ms, applying a voltage of ~25 kV from EN1 to the discharge gap. The stored energy in EN-1 was ~4 kJ. Immediately after voltage application, a high-current arc discharge occurred; oscillograms of current and voltage across the discharge are shown in Fig. 4. The maximum discharge current value was 90 kA, the current rise rate at the initial moment was 20 kA/μs, the period of damped oscillations of current and voltage T_a ~20 μs.

Special experiments were conducted to evaluate the dynamics of hydrogen concentration growth after opening the valves by measuring the breakdown voltage of a model gap with 6 mm distance between electrodes [20]. It was shown that decreasing the applied voltage increased the breakdown delay time. This indicates that the breakdown voltage decreased with increasing hydrogen concentration, which corresponds to the left branch of the Paschen curve [21]. From these experiments, it was determined that by the time voltage was applied to the discharge gap, the hydrogen molecule concentration was $n_m \sim 3 \cdot 10^{16}$ cm^{-3}. According to estimates, during the discharge burning time (~0.1 ms), the concentration increased to $\sim 4 \cdot 10^{16}$ cm^{-3}.

Figure 4 also shows the solenoid current at a charging voltage of EN-2 10 kV: maximum current – 87 kA, its oscillation period ~60 μs. The amplitude value of the current in the solenoid was proportional to the charging voltage of EN-2, so at a voltage of 15 kV, the maximum current was equal to ~150 kA.

Using the Elcut program [22], modeling of the magnetic field created by the solenoid in the discharge gap was carried out. The model did not account for the influence of the current in the plasma, which distorted the external field. At the maximum current in the solenoid of 200 kA, the magnetic induction across the discharge gap increased in the direction from cathode to anode from 3 to 7 T. The change in magnetic induction along the electrode surface inside the solenoid did not exceed 10%. Below are the calculated values of magnetic induction in the middle of the discharge gap B_{av}. For the mode presented in Fig. 4, at the maximum current in the solenoid B_{av} =2.3 T.

Fig. 5 shows the development of plasma formation in the absence of an external magnetic field (in the frames, the dark circle on the right is the TZL). Under each frame, the time elapsed since the breakdown and the discharge current are shown.

It can be seen that after ~5 μs after breakdown, relatively symmetrical near-surface layers are formed, after ~8 μs the plasma already fills the space in front of the central electrode, after ~10 μs its maximum glow is achieved, which extinguished ~0.2 ms after appearance. Figure 6a, b shows the plasma parameters measured in the discussed experiment using a Langmuir probe, which was installed near the inlet valve. Recording of probe characteristics began ~10 μs after the breakdown of the discharge gap. The characteristic values of electron temperature and electron density were ~2 eV and ~$2 \cdot 10^{13}$ cm $^{-3}$ respectively; Figure 6a also presents a "calculation" of electron temperature, with the calculation methodology given in Section 4.

Figure 7 shows the averaged spectrum of hydrogen plasma recorded in the discussed experiment; the "inset" in the upper part of this figure shows a fragment of the spectrum taken with a Phantom VEO710 camera. The electron temperature, calculated using formula (3) based on the averaged intensities of H α and H β lines, was ~1.5 eV.

The value of electron density n_e, estimated from the half-width of the H β line profile, averaged over the recording time by the monochromator with a Toshiba1304 camera, according to formula (4), was $n_e \approx 1.3 \cdot 10^{14}$ cm $^{-3}$.

The following discusses the influence of the magnetic field on the plasma clot, which was created by a solenoid at an EN2 voltage ranging from 5 to 20 kV, when the maximum value of the average induction B_{av} varied from 1.5 to 7 T.

Figure 8 shows high-speed photography frames illustrating the dynamics of discharge development with the application of a magnetic field, with charging voltage of EC2 at 10 kV. For each frame, the time elapsed since the beginning of the discharge, the discharge current, and the average value of the magnetic field induction B_{av} are provided. Negative values of B_{av} correspond to a change in the current direction in the solenoid. Comparing Fig. 5 and 8, it is evident that the magnetic field significantly affected the shape of the plasma formation, which acquired a toroidal form that persisted until the luminescence disappeared, which occurred approximately 70 μs after the discharge initiation. Unlike the mode without a magnetic field, the plasma formation did not overlap the central electrode, as evidenced by the absence of luminescence in front of it. In the range of EC2 charging from 5 to 20 kV, the dynamics of the plasma formation at a qualitative level remained the same as shown in Fig. 8.

Figures 9 and 10 show the results of plasma parameter measurements at two values of EC2 charging voltage; the Langmuir probe in both cases was located at a distance of ~15 mm from the inlet valve. As can be seen, with an increase in the magnetic field induction, there is a tendency for electron concentration to increase while their temperature decreases.

For the correct application of the Langmuir probe, it is necessary that the thickness of the space charge layer near its surface, determined by the Debye radius, be much smaller than the probe diameter [21]. With the measured values of electron concentration and their temperature, the Debye radius was estimated to be $\sim 10^{-3}$ cm, which is two orders of magnitude smaller than the probe diameter.

The presented results were obtained using a single gas inlet valve. The simultaneous use of multiple valves allows increasing the mass of the plasma-forming gas, but to maintain or even increase its ionization degree, it is necessary to raise the energy of the capacitive storage ES1. This is planned for the next stage of research. Nevertheless, it should be noted that preliminary results were obtained on igniting the discharge when using a larger number of valves, and a scheme for their simultaneous activation was developed. These experiments showed that when using three to six valves, a symmetrical and homogeneous plasma clump with distinct boundaries at the electrode surface forms almost immediately at the moment of discharge ignition in the interelectrode gap. However, as expected, the electron concentration was lower than when using a single valve.

4. DISCUSSION OF THE OBTAINED RESULTS

From Fig. 4, it follows that the investigated discharge is characterized by relatively weak attenuation. Table 1 shows the values of local extrema of current, voltage on the discharge at the

moment of extrema, and the resistance of the discharge gap R_a. Voltage extrema preceded current extrema by ~3 μs. As can be seen, during the discharge time, the current value at local extrema decreases by an order of magnitude, while the voltage changes by only ~50%. If we neglect near-electrode potential drops, the average value of the electric field strength in the interelectrode gap E for the modes presented in Table 1 varied from 25 to 35 V/cm.

As can be seen, the period of damped current oscillations T_a remained practically constant, which means a small change in the circuit inductance L. If the value of the active resistance of the circuit R_0 can be assumed constant, then the discharge current is determined from the relation [24]

$$I(t) = q_0 \frac{\omega_0^2}{\omega} \exp(-\gamma t) \sin(\omega t) \qquad (5)$$

Where $q_0 = CV_0$ is the charge of ES, other parameters are determined from the relations

$$\omega_0 = 1/\sqrt{LC} \qquad (6)$$

$$\gamma = R_0/(2L) \qquad (7)$$

$$\omega = \sqrt{{\omega_0}^2 - \gamma^2} = 2\pi/T_a \qquad (8)$$

Table 1. Discharge parameters at local current extrema

Extremum time, μs	Current extremum, kA	Voltage, kV	Resistance R_a, mOhm	Resistance R_0, mOhm
410	90	-0.15	1.6	420
420	-75	0.15	2.0	8.1
430	53	-0.15	2.8	15
440	-45	0.12	2.7	7.2
450	31	-0.15	4.8	17
460	-26	0.12	4.7	7.5
470	17	-0.099	5.8	19
480	-15	0.099	6.6	5
490	8.3	-0.099	12	26

From the current oscillogram in Fig. 4 and relations (6), (8), it follows that the circuit inductance L was equal to 0.87 μH ($\gamma << \omega$, C =12 μF). Table 1 shows the total circuit resistance R_0, which was estimated using formula (5) for consecutive current extrema. As can be seen from Table 1, in the cathode polarity of the central electrode, the circuit resistance (R_0) is significantly lower than in the anode polarity.

The nature of plasma movement in the MPC was very complex, influenced by the swirling hydrogen flow, whose velocity was probably comparable to the speed of sound in it – 1.3 km/s (1.3 mm/μs). In the absence of an external magnetic field, plasma movement was also determined by the pressure gradient and ponderomotive forces of the discharge current. Under the influence of these forces, the plasma clump moved along the electrode surface, and about ~8 μs after discharge initiation, its glow overlapped the central electrode (see Fig. 5). From this it follows that if the breakdown occurred opposite the inlet valve, then the plasma flow velocity was ~25 km/s. This value is an upper estimate of the plasma velocity u_p, since the discharge could have occurred closer to the outlet section of the central electrode. Subsequently, apparently, the zone of this electrode was alternately the cathode or anode of the discharge, and the attachment zone on the outer (return) electrode slid along its inner surface, increasing the length of the discharge. This nature of discharge expansion explains the tendency for its resistance to increase (see Table 1).

Note that the electron concentration, estimated from the broadening of the H_β line, is approximately an order of magnitude higher than that measured by TLP. This allows us to conclude that the results presented in Fig. 6 were obtained at the periphery of the discharge, where its current density is relatively low. From the data in Figure 4, the average value of the electric field in the interelectrode gap E is found, and then - the Townsend parameter E / n_m [21], for the concentration of hydrogen molecules n_m a value of $3 \cdot 10^{16}$ cm^{-3} was assumed. In reference [23], the drift velocity u_e and electron temperature are given as functions of the Townsend parameter. Based on these data, the electron temperature shown in Fig. 6 was calculated. As can be seen, the calculated temperature values are consistent with the results of TLP measurements. According to Fig. 6, the characteristic electron temperature during the discharge was about 2 eV; at such an electron temperature, their drift velocity is $\sim 6 \cdot 10^6$ cm/s [23]. From the drift velocity, the constant of elastic collisions of electrons with hydrogen molecules k $k_{em} \sim 1.5 \cdot 10^{-7}$ cm^3/s and the frequency of elastic collisions of electrons with them $\nu_{em} = k_{em} n_m \sim 5 \cdot 10^9$ s^{-1} are determined.

The picture of the plasma clot motion changes significantly when an external magnetic field is applied, which can either accelerate or decelerate it. The plasma motion in the central region of the solenoid, where the electric and magnetic fields are perpendicular to each other, is described relatively simply. Here, charged particles drift in a direction perpendicular to both fields. The electron velocity in the plasma u is determined from the solution of the equation [24]

$$m_e \dot{u} = -\mathrm{e}(E + [\bar{u} \times B]) m_e u \nu_{\mathrm{eg}} \qquad (9)$$

where v_{eg} is the collision frequency of electrons with heavy particles. From equation (9), the projections of the electron velocity u_n and u_t, directed perpendicular to the electrode surface (parallel to the field E) and around the central electrode, respectively, are found

$$u_n = -\frac{eE}{m_e \nu_{eg}(1+\beta^2)} \quad (10)$$

$$u_t = -\frac{eE\beta}{m_e \nu_{eg}(1+\beta^2)} \quad (11)$$

where β is the Hall parameter [21] $\beta = \frac{\omega_B}{\nu_{eg}}$

The cyclotron frequency of electrons ω_B is determined from the relation

$$\omega_B = eB/m_e \quad (12)$$

Electrons rotate around the central electrode with velocity u_t; when its polarity changes, the rotation velocity changes to the opposite direction; such a motion pattern may contribute to the formation of toroidal plasma structures. The change in rotation direction possibly affects the discharge resistance and, consequently, the resistance of the entire circuit R_0 (see Table 1). From comparing the formulas for u_n and u_t it is evident that when $\beta > 1$, the velocity of electrons directed from cathode to anode is less than their rotation velocity around the central electrode.

As follows from (10) and (11), the electron velocity depends on the Hall parameter. With a characteristic magnetic field induction value of ~1 T, the cyclotron frequency ω_B equals $\sim 2 \cdot 10^{11}$ rad/s. If the Hall parameter is estimated using the above value of the electron collision frequency with hydrogen molecules ν_{em} ($\sim 5 \cdot 10^9$ s^{-1}), then the parameter $\beta \sim 30$. This estimate is valid for the periphery of the discharge, where the ionization degree is small; in its central zone, electron scattering also occurs on ions, so the value of the Hall parameter in this zone will be smaller. Apparently, under the conditions of the presented experiments, during the discharge time, the average value of parameter β exceeded unity. From formula (9), it can be seen that the external magnetic field reduces the drift velocity u_n, therefore, with the same discharge current, an increase in this field should be accompanied by an increase in the electron concentration and, consequently, an increase in the ionization rate, which should lead to a decrease in the electron temperature. This circumstance possibly explains the tendency noted in Section 3 of increasing electron concentration while decreasing their temperature with increasing magnetic field induction (Fig. 9). A similar dependence of plasma parameters on the external magnetic field was obtained in works [25, 26].

5. CONCLUSIONS

The performed studies allow us to draw the following conclusions.

1. The proposed design of multi-channel injection allows increasing the mass of plasma-forming gas, however, to increase its ionization degree, it is necessary to raise the energy supplied to the discharge. Preliminary results showed that using a larger number of inlet valves makes it possible to obtain a more uniform plasma bunch.

2. It is shown that the application of an external magnetic field allows stabilizing the plasma bunch, giving it a toroidal geometry, with estimates of the Hall parameter ranging from ~5 to ~30.

3. Plasma parameters can be controlled by changing the magnitude of the magnetic field and the delay time between the current extrema in the discharge and solenoid.

4. The tested multi-channel injection system can be used for initial plasma acceleration at the inlet of a pulsed plasma accelerator.

5. The measurements performed with a triple Langmuir probe showed that it is a convenient tool for monitoring plasma parameters in a pulsed arc discharge. It was demonstrated that an increase in the magnetic field induction is accompanied by an increase in electron concentration with a decrease in their temperature.

FUNDING

The work was carried out at the Joint Institute for High Temperatures of the Russian Academy of Sciences within the framework of budget funding, State registration number in USRDT 122031400708-4. The work was also supported by the Ministry of Science and Higher Education of the Russian Federation (State Assignment No. 075-00269-25-00).

REFERENCES

1. *Kutukov A.K., Panin S.E., Podkovyrov V.L., Sergeechev A.A., Baibakov G.S., Petrakov M.V., Mamonov A.A.* // Engineering Physics. 2023. No. 10. P. 47. DOI: 10.25791/infizik.10.2023.1362

2. *Panteleenko F.I., Okovity V.A., Devoino O.G., Volodko A.S., Sidorov V.A., Okovity V.V., Litvinko A.A., Astashinsky V.M.* // Progressive Technologies and Systems of Mechanical Engineering. 2023. No. 1 (80).

3. *Gavrilov V.V., Eskov A.G., Zhitlukhin A.M., Kochnev D.M., Pikuz S.A., Poznyak I.M., Ryazantsev S.N., Skobelev I.Yu., Toporkov D.A., Umrikhin N.M.* // Plasma Physics. 2020. Vol. 46. No. 7. P. 606. DOI: 10.31857/S0367292120070045.

4. *Toporkov D.A., Burmistrov D.A., Gavrilov V.V., Zhitlukhin A.M., Kostyushin V.A., Lidzigoriaev S.D., Pushina A.V., Pikuz S.A., Ryazantsev S.N., Skobelev I.Yu.* // Plasma Physics 2023. Vol. 49. No. 8.

DOI: 10.31857/S0367292123600358

5. *Bannov S.G., Zhitlukhin A.M., Motorin A.A., Stupitsky E.L., Kholodov A.S., Cherkovets V.E.* // Geomagnetism and Aeronomy. 2019. Vol. 59. No. 3. P. 340. DOI: 10.1134/S0016794019030039.

6. *Dudin S.V., Kozlov A.V., Shurupov A.V., Zhitlukhin A.M., Leontiev A.A., Mintsev V.B., Ushnurtsev A.E., Fortov V.E., Cherkovets V.E., Shurupova N.P.* // TVT . 2010. Vol. 48. No. 1 . P. 3. DOI: 10.1134/S0018151X10010013.

7. *Kovalenko D.V., Klimov N.S., Zhitlukhin A.M., Muzychenko A.D., Podkovyrov V.L., Safronov V.M., Yaroshevskaya A.D.* // VANT. Ser. Thermonuclear Fusion. 2014. No. 4. issue 37. p. 39.

8. *Kostyushkin V.A., Poznyak I.M., Toporkov D.A., Burmistrov D.A., Zhuravlev K.V., Lidzigoriaev S.D., Usmanov R.R., Tsybenko V.Yu., Nemchinov V.S.* // PTE. 2023. No.6. P.28.

9. *Umrikhin N. M.* Dissertation... Candidate of Physical and Mathematical Sciences. Moscow: IAE named after I.V. Kurchatov, 1984.

10. *Kozlov A.V., Mashtakov A.V., Shurupov A.V., Gusev A.N., Zavalova V.E., Shurupov M.A, Shurupova N.P., Zhitlukhin A.M., Bakhtin V.P.* // TVT. 2022. No.3. Issue 60. P. 331. DOI: 10.31857/S0040364422010306.

11. *Sivkov A.A., Isaev Yu.N., Vasilyeva O.V., Kuptsov A.M.* // Proceedings of Tomsk Polytechnic University. 2010. vol. 317. Issue 4. P. 74.

12. *Voronin A.V., Gusev V.K., Kobyakov S.V.*, //ZhTF. 2011. vol.81. issue 7. p. 63.

13. *Novikov Ya.V., Roslyakov I.A., Frolov A.Yu., Eskov A.G., Zhitlukhin A.M., Umrikhin N.M.* Plasma accelerator with magnetic gate. Utility model patent. RU 188484 U1. 2019

14. Gusev A.N., Kozlov A.V., Shurupov A.V., Mashtakov A.V., Shurupov M.A. // PTE. 2020. No.1. P.1. DOI: 10.31857/S0032816220050146

15. *Naz M.Y., Shukhrulla S., Jafar A., Rehman N.U., Khan Y. //* PMTF. 2016. V.57. No.2. P.23. DOI: 10.15372/PMTF20160203.

16. *Lochte-Holtgreven W.* Methods of Plasma Investigation. Moscow: Mir Publishing. 1971.

17. *Semiokhin I.A*. Elementary Processes in Low-Temperature Plasma. Moscow: Moscow University Publishing. 1988.

18. *Sobelman I.I.* Introduction to the Theory of Atomic Spectra. Moscow: Fizmatgiz, 1963.

19. *Kasabov G.A., Eliseev V.V.* Spectroscopic Tables for Low-Temperature Plasma. Moscow: Atomizdat, 1973, 160p.

20. *Zavalova V.E., Kozlov A.A., Kozlov A.V., Polistchook V.P., Karpushin Yu.V., Shurupov M.A.* // EFRE-2024: 9 th International Congress on Energy Fluxes and Radiation Effects (EFRE-2024): Abstracts. Tomsk: Academizdat Publishing, 2024., C1-P-023104, ISBN 978-5-6052421-8-5.

21. *Raizer Yu.P.* Gas Discharge Physics. Moscow: Nauka, 1987. 592 p.

22. https://elcut.ru/about . ELCUT Student. distributed free of charge

23. Physical Quantities. Reference Book / Ed. by Grigoryev I.S., Meilikhov E.Z. Moscow: Energoatomizdat, 1991.

24. *Sivukhin D.V.* General Course of Physics. Electricity. Moscow: Nauka, 1977.

25. *Borthakur S., T alukdar N., Neog N. K., and Borthakur T. K.* // Physics of Plasmas. 2018. V.25. DOI: 10.1063/1.5009796

26. *Meng L., Cloud A. N., Jung S., and Ruzic D. N.* // J. Vac. Sci. Technol. 2011. V 29. DOI: 10.1116/1.3528940.

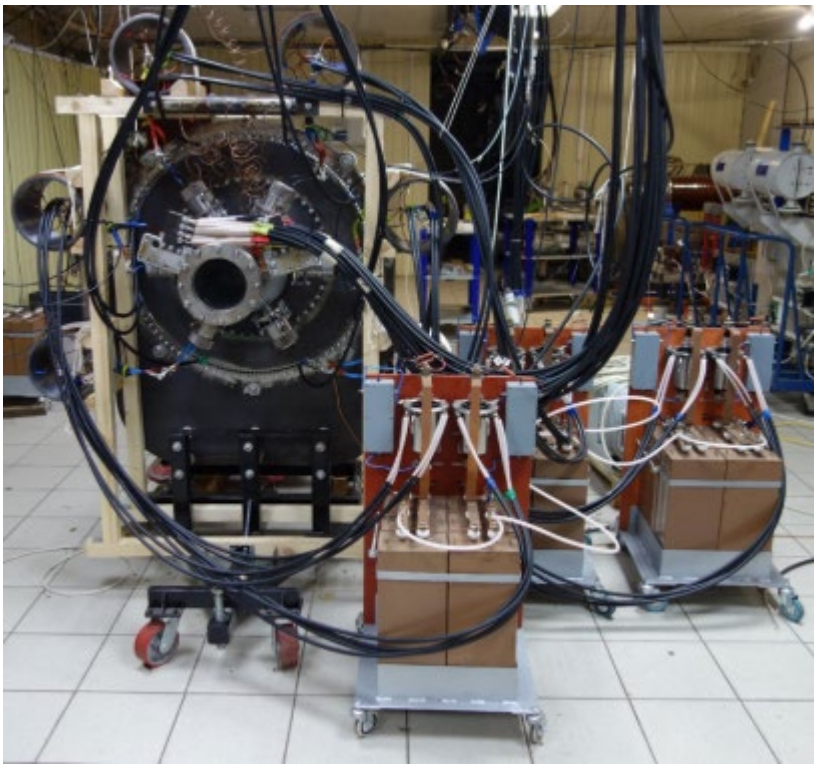

Figure 1 - Photo of the MCI model

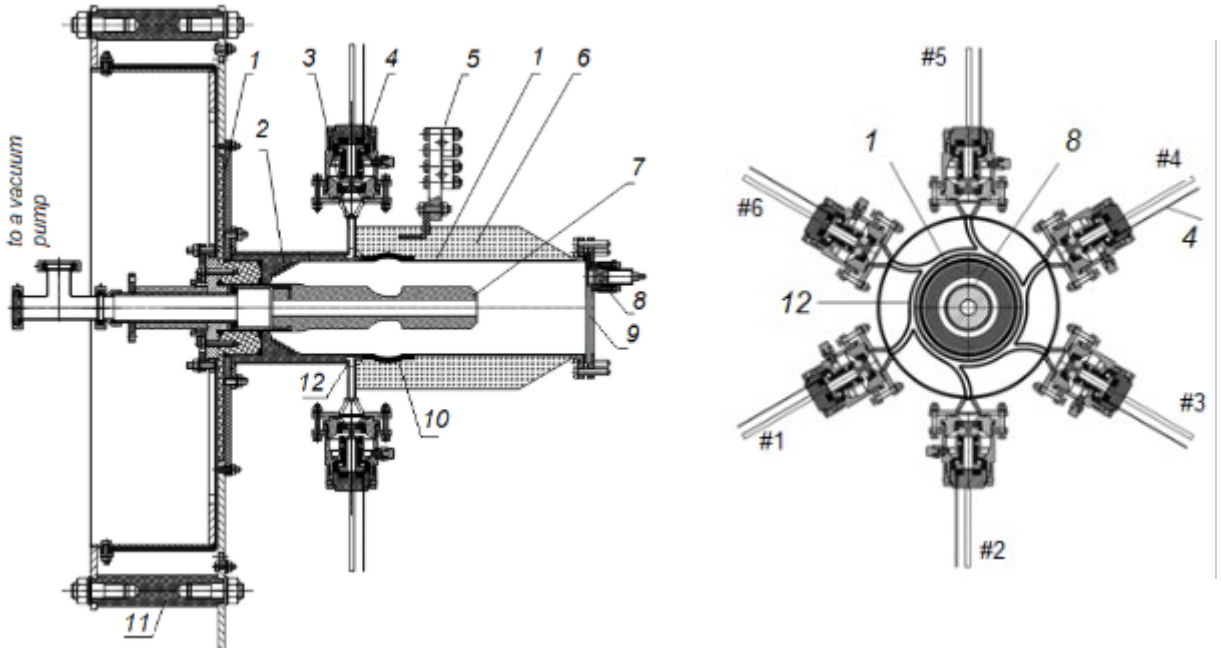

a) b)

Figure 2 - Sketch of the MCI model in longitudinal a) and transverse b) sections.
Structural elements: 1 - outer electrode (anode); 2 - insulator with developed surface; 3 - electrodynamic gas inlet valve; 4 - valve rod trigger wire; 5 - solenoid power collector; 6 - banding; 7 - central electrode (cathode); 8 - socket with bracket for probe installation; 9 - flange with Wilson seal (replaceable with acrylic viewing window); 10 - solenoid; 11 - current collector; 12 - working gas mixer.

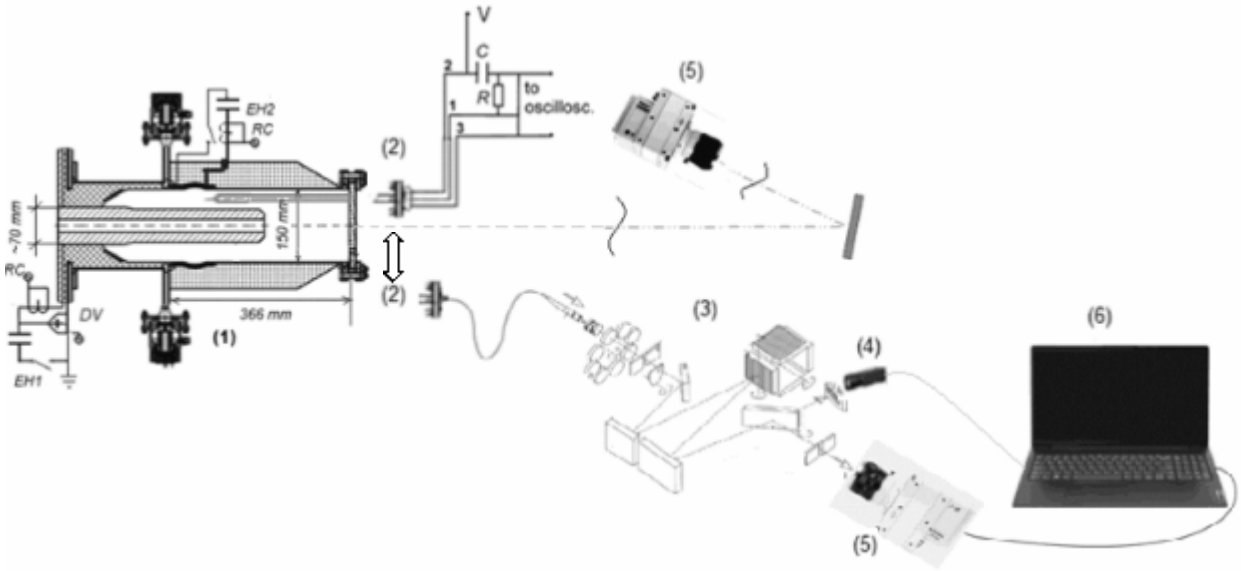

Figure 3 Measurement schemes. Where: EN1 and EN2 - capacitive storage units; RC - Rogowski coils; DV - voltage divider; (1) - MCI IPU model; (5) - Phantom VEO-710 video camera . For spectral measurements: (2) - matching optics, outputting radiation through fiber optic cable to monochromator (3) and through the main port to Toshiba1304 camera (4) or through an additional port to Phantom VEO-710 (5), and to (6) - PC. For probe measurements (2) - this is the probe insertion through the output flange of the model and the electrical connection diagram of the LTP.

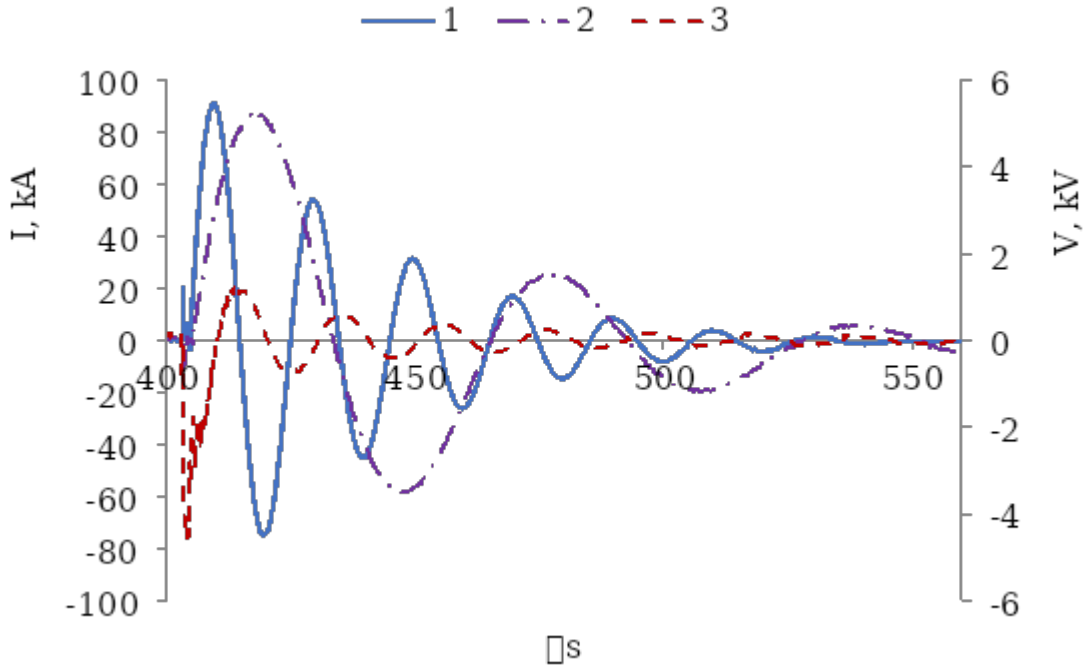

Figure 4 - Oscillograms: discharge current 1 *1* , solenoid current - *2* , discharge voltage 3 *3* .

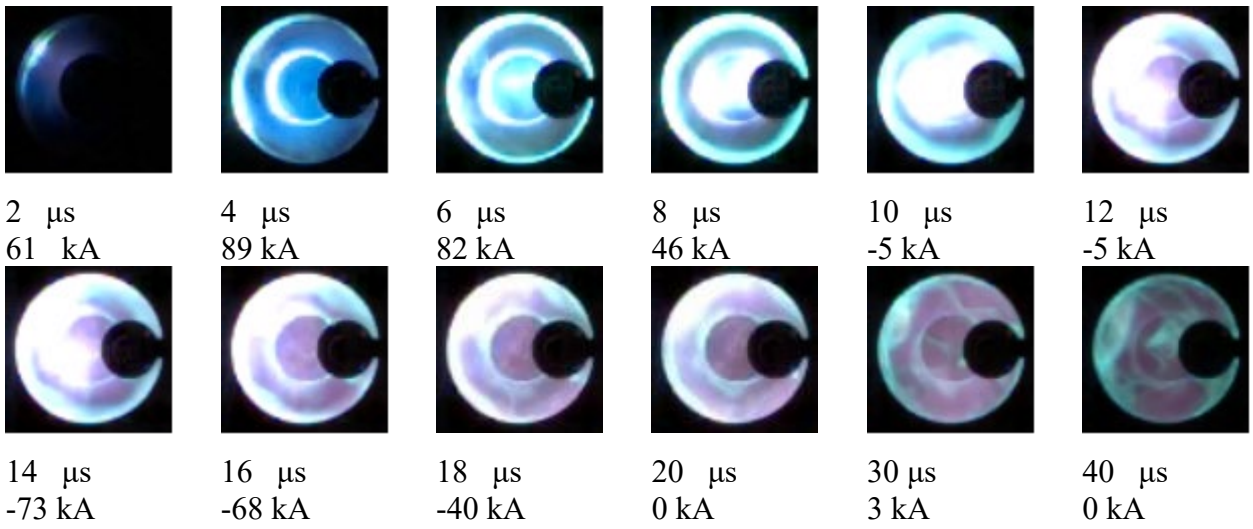

Figure 5 – Dynamics of the plasma shell in the absence of an external magnetic field.

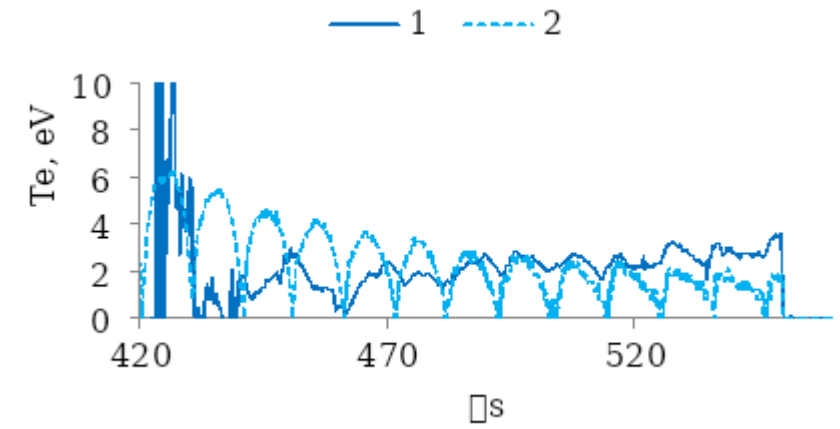

-a-b-

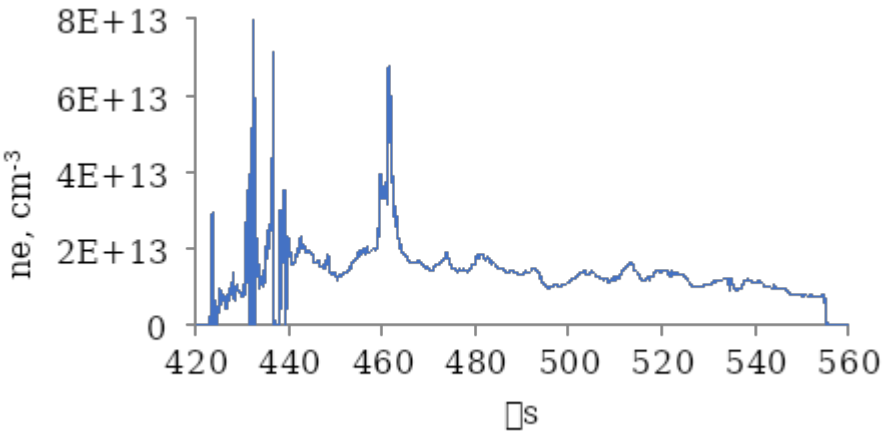

-б-

Figure 6 – Plasma parameters in the absence of an external magnetic field:
a – Electron temperature, measured (1) and "calculated" (2);

b – Electron concentration.

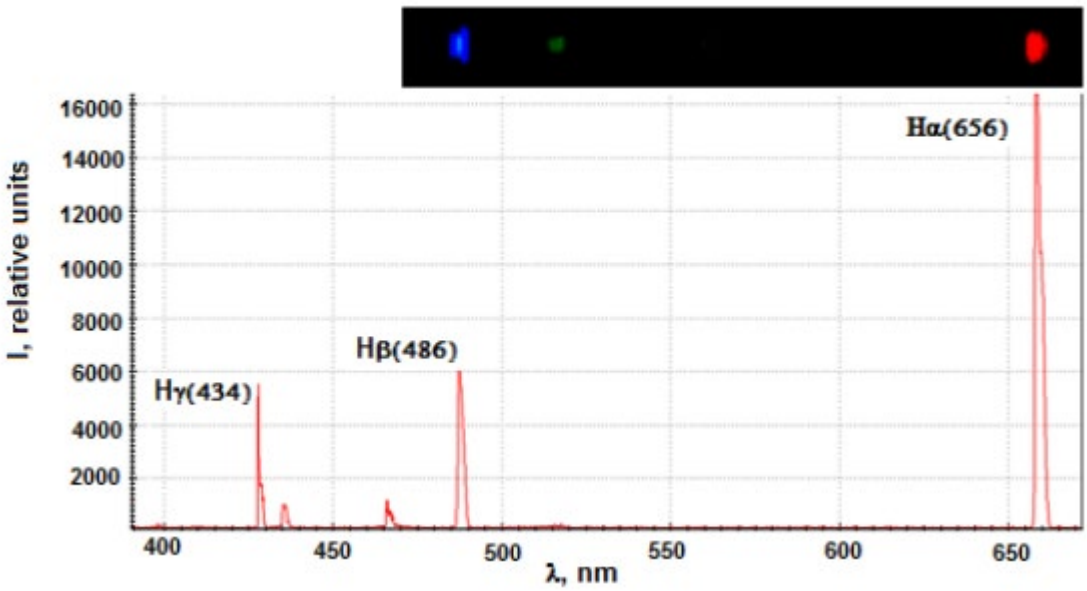

Figure 7 – Measured emission spectrum of hydrogen plasma.

			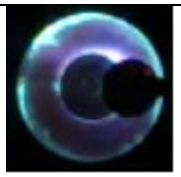	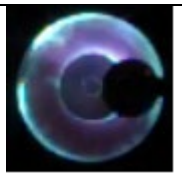	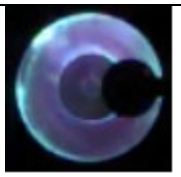
2 μs 62 kA 0.5 T	4 μs 90 kA 1.0 T	6 μs 82 kA 1.5 T	8 μs 45 kA 1.8 T	10 μs -5 kA 2.0 T	12 μs -5 kA 2.2 T
					
14 μs -72 kA 2.2 T	16 μs -70 kA 2.1 T	18 μs -40kA 1.9T	20 μs 0 kA 1.6T	30 μs 3kA -0.3 T	40 μs 0 kA -1.4 T

Figure 8 – Dynamics of the plasma bunch in an external magnetic field.

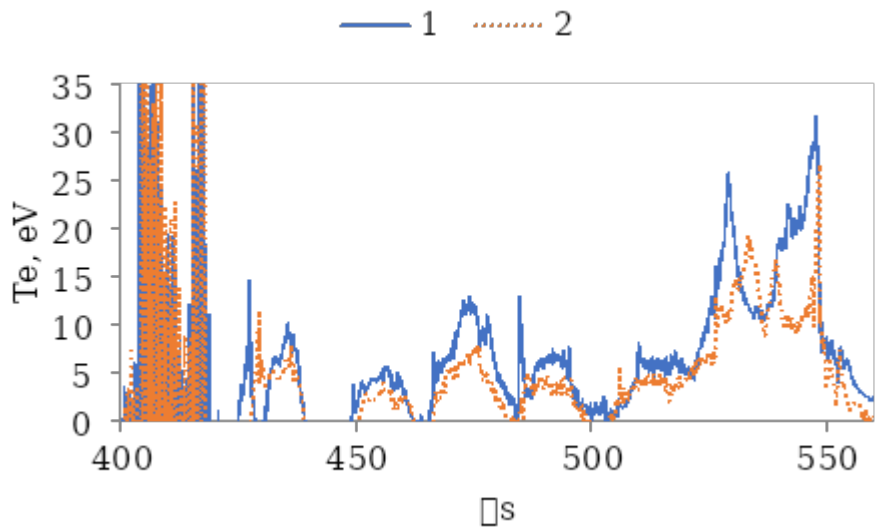

(a)

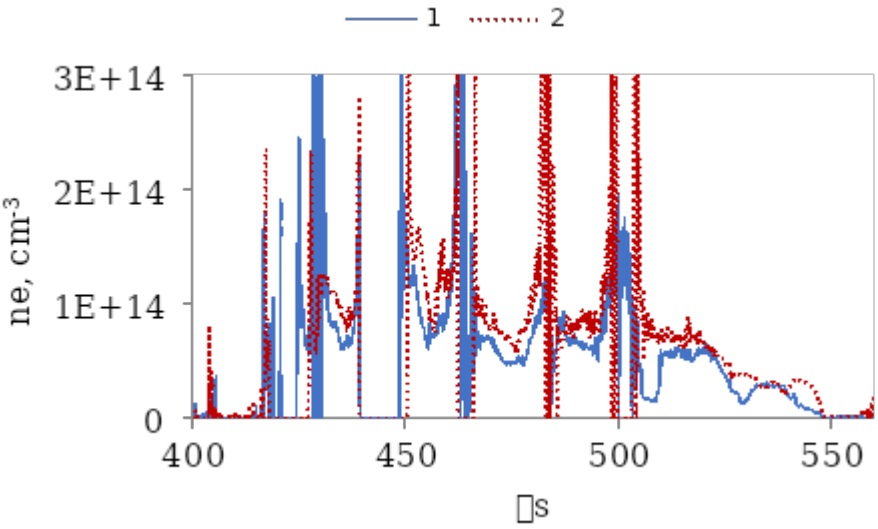

-(b)Figure

9 – Changes in electron temperature (a) and their concentration (b) in the plasma bunch at charging voltage EC2 10 kV *1* and 15 kV *2* .